Modulation of Absorption in Field-Effect Quantum Well Structures

D. S. CHEMLA, MEMBER, IEEE, I. BAR-JOSEPH, J. M. KUO, T. Y. CHANG, MEMBER, IEEE, C. KLINGSHIRN, GABRIELA LIVESCU, AND DAVID A. B. MILLER

(Invited Paper)

Abstract—**We present experimental and theoretical investigations of the absorption in a single modulation-doped quantum well (QW) used as conducting channel of a field-effect transistor. By applying a voltage to the gate, the electron concentration can be varied between 0 and $\approx 10^{12}$ cm^{-2}. We can thus follow optically the continuous transition from an undoped to a highly doped QW. We observe effects of band filling and renormalized at the first subband edge and electrostatic effects at the higher ones. We show that optical techniques can give *in situ* information on the electron density and temperature as well as on the electrostatic fields inside field-effect structures. Finally, since the quenching of the absorption can be total, we comment on the potential applications of this effect to high-speed modulators and optical interconnects for III–V electronics.**

I. INTRODUCTION

RECENTLY, the nonlinear optical properties of undoped semiconductor quantum well structures (QWS's) have attracted much attention because of their potential applications in optoelectronics. Indeed, large changes in the absorption coefficient and refractive index of undoped QWS's have been demonstrated at room temperature, either by photoexcitation [1] or by application of electrostatic field (parallel or perpendicular to the plane of the quantum well) [2], [3]. These unusual properties are due to quantum size effects, which produce major modifications of the near-bandgap interaction of light with ultrathin semiconductor layers. In this region, the linear as well as the nonlinear optical properties of QWS's are significantly different from those of the bulk parent materials. First, the linear absorption spectrum is modified by the confinement of electrons and holes (e–h) in the QW. The quantization of the motion of the carriers perpendicular to the layer produces a series of two-dimensional (2-D) subbands (customarily labeled by a quantum number n_z). Consequently, the joint density of states that governs the optical transitions has a step-like structure. Furthermore, by artificially reducing the e–h average distance, the confinement reinforces their interaction, hence giving more tightly bound excitons. This results in strong excitonic resonances at the onset of each intersubband transition [4]. These excitons remain well resolved even at room temperature [5]–[7]. The mechanisms governing nonlinear effects due to photocarriers in QW's are also different from the corresponding ones in bulk materials. The reduced dimensionality diminishes the efficiency of the long-range direct Coulomb screening of the e–h interaction. The presence of an e–h plasma in the QW only affects the excitons through the short-range phase-space filling (PSF) and Coulomb exchange interaction, both of which are consequences of the exclusion principle [8]. Electroabsorption in the QWS is especially unusual when the electric field is directed perpendicular to the layers. Since the height of the potential discontinuities between the QW and the surrounding material can be more than one order of magnitude larger than the depth of the e–h Coulomb well, large electric fields can be applied perpendicular to the QW, inducing large Stark shifts of the exciton resonances without significant field ionization [2], [3]. This effect is known as the quantum confined Stark effect (QCSE). It depends critically on the thickness L_z of the QW and continuously transforms into the normal Franz–Keldysh effect when L_z becomes much larger than the bulk-exciton Bohr radius a_0 [9].

Modulation-doped (MD) QW's [10] have been extensively studied in electronic transport [11] and magnetotransport [12] owing to their extremely high mobilities. The MD-QW's are fabricated by introducing the doping impurities in the barrier layers during the growth, hence spatially separating them from the mobile carriers, which fall in the lower-gap QW. Until recently, the optical properties of MD-QW's have been investigated less intensively, although they are extremely interesting in their own right. The most striking features of the absorption and emission behavior are the following. The occupation of the conduction (valence) subbands by the 2-D electron (hole) gas produces a blue shift of the absorption edge similar to the Burstein–Moss effect seen in bulk materials. However, exciton resonances are found to persist at the onset of the high-energy intersubband transitions ($n_z = 2$, 3), despite the very large carrier concentration within the QW. Nevertheless, the carriers introduced by the modulation doping can participate in luminescence, which thus still starts at the $n_z = 1$ intersubband gap [13]. In addition, the presence of a Fermi sea produces several interesting many-body effects in the optical response of MD-QWS's. For example, the bandgap is renormalized so that

Manuscript received December 22, 1987; revised March 14, 1988.

D. S. Chemla, I. Bar-Joseph, J. M. Kuo, T. Y. Chang, G. Livescu, and D. A. B. Miller are with AT&T Bell Laboratories, Holmdel, NJ 07733.

C. Klingshirn was with AT&T Bell Laboratories, Holmdel, NJ 07733. He is now with Fachbereich Physik, Universität Kaiserslautern, D6750 Kaiserslautern, Germany.

IEEE Log Number 8821716.

the $n_z = 1$ luminescence edge is red shifted [14], [15]. The luminescence in n-type MD-QWS's exhibits yet another many-body effect, seen in the polarization characteristics of the emission spectra. It is found that the heavy-hole (hh) ($M_z = \pm 3/2$) subband is significantly mixed with the light-hole (lh) ($M_z = \pm 1/2$) subband, even at $k = 0$ [16], [17]. This mixing is induced by a "shakeup" of the Fermi sea, analogous to that observed in X-ray emission [18]. As a consequence of the correlation between the whole Fermi sea and the hole, singularities appear near the Fermi energy E_F, producing a strong enhancement of the optical transitions in the vicinity of this energy [19]. They have been observed in luminescence (to a localized hole state) [20] and directly in absorption as well [13], [21].

It is clear from the above discussion that it would be very interesting to be able to drive electrons in and out of a QW in a controlled manner. From a fundamental point of view, this would enable us to investigate the modification of the optical properties brought about by the presence of carriers. It would thus be possible to compare directly the electronic structures of the two types of QW's, while avoiding all the parameter fluctuations that arise when comparing different samples. Furthermore, we can anticipate that large changes in the absorption will occur, especially close to the gap. These could be exploited for application to optoelectronic devices. We have recently shown that it is indeed possible to achieve such control, electrically, in field-effect (FE) QWS's [22], [23]. In such structures, a gate electrode is placed above the MD-QW, and the carrier concentration in the well is changed by application of voltage to the gate, thus varying the width of the depletion layer beneath it. Using this technique, it is possible to follow optically, through the changes in the absorption spectrum, the continuous transition from an undoped QW to a highly doped MD-QW.

In this paper, we review our investigations of the optical properties of FE-QWS's [22], [23]. We have found that optical absorption spectroscopy techniques provide direct *in situ* information on the electronic structure of the QW as well as on thermodynamic parameters of the 2-D electron gas. Both types of information are important for understanding the physics of FE devices. The changes in the optical parameters are very large and can be used for efficient intensity and/or phase modulation of the light passing through the FE-QWS. Finally, since the optical parameters measure directly the concentration of carriers in the FE-QWS, they can be used to read optically the logic state of field-effect transistors (FET's), in which the conducting channel is a QW. This effect has potential applications for optical interconnections of III–V electronics. Control of the carrier concentration using this technique has recently been used in GaAs FE-QWS to investigate the density dependence of emission characteristics [24], [25].

The paper is organized as follows. In Section II, we give a quantitative discussion of the absorption spectra of undoped and MD-QW's and briefly introduce all the concepts and notations necessary for the rest of the paper. In Section III, we describe our experimental investigation of the modulation of absorption in n-type InGaAs/InAlAs FE-QWS's and in Section IV, we give a detailed interpretation of the most salient features. Finally, in the conclusions, we discuss the potential applications of these effects.

II. Absorption in Undoped and Modulation-Doped QW's

A. Undoped QW's

The optical absorption spectra of undoped QWS's are now well understood [26], [27]. In this subsection, we will briefly recall the main results.

It is instructive to consider first the idealized case of an infinitely deep QW made of a semiconductor with nondegenerate parabolic bands. The quantization of the motion in the direction perpendicular to the QW, which we take as the z-axis, gives rise to confined levels with energies: $E^{\infty}_{e,h}(n_z) = (\hbar^2/2m_{e,h}) \times (\pi n_z/L_z)^2$ where m_e and m_h are the e–h effective masses. Since the particles are free to move along the plane of the layer, the joint density of states that governs the optical transitions consists of a series of steps obeying the selection rule $\Delta n_z = 0$. The absorption spectrum is modified by the e–h Coulomb interaction, which produces a hydrogenic series of excitonic peaks below each intersubband edge and a correlation enhancement (the so-called Sommerfeld enhancement) in the continua [28]. The excitonic bound states are naturally labeled by the discrete quantum number $n = 1, 2, \cdots$ that defines the energies of the 2-D Balmer series; $E_n = -R_y/(n - 1/2)^2$ where R_y is the Rydberg constant of the material. Correspondingly, the scattering (unbound) states can be labeled by a quantum number p, with a continuous spectrum. For each intersubband transition, the high-energy exciton states ($n >> 1$) form a quasi-continuum that merges continuously into the true continuum (p), thus giving a smooth transition in the absorption profile [28].

To describe the case of real quantum wells, one has to account first for the finite height of the potential barriers in the conduction (c) and valence (v) bands $\Delta E_{c,v}$. In this case, the quantization of the motion perpendicular to the wells gives only a limited number of confined states in each band and continua of delocalized states. The confined states are less bound than in the infinite well, $E_{e,h}(n_z) < E^{\infty}_{e,h}(n_z)$, and their number is equal to the number of states in the infinite well with energy smaller than $\Delta E_{c,v}$. They can still be labeled by the quantum number n_z, which now determines the number of nodes, $(n_z - 1)$ of the wave function. Furthermore, because of the difference of masses and potential barriers the e and h wave functions do not penetrate equally in the barrier material. This causes a breakdown of the $\Delta n_z = 0$ selection rule. However, the $n_{e,z} \neq n_{h,z}$ transitions remain usually weak and are often referred to as "forbidden transitions." A further complication arises from the complex structure

of the valence subbands of III–V semiconductors. Without getting into the details of the in-plane dispersion of the hole states [29]–[31], we can consider that the main result of the confinement is to lift the degeneracy of the valence bands. Accordingly, two series of exciton resonances should appear, associated with the hh and the light hole lh, respectively. In actual samples, the ideal absorption profile described above is blurred by unavoidable imperfections (fluctuations in the layer thickness, strain due to small lattice mismatch, interface defects), as well as by intersubband coupling and temperature broadening. As a result, only the hh and lh exciton ground states are resolvable at the lowest absorption edge. It has been found that the experimental absorption profile of undoped QW, $\alpha^{(0)}(\hbar\omega)$, is well fitted by a semiempirical formula [32]:

$$\alpha^{(0)}(\hbar\omega) = \sum_{n_z} \left(\alpha^{(0)}_{X,n_z}(\hbar\omega) + \alpha^{(0)}_{C,n_z}(\hbar\omega)\right). \quad (1)$$

In this expression, the sum runs over n_z, and the contributions of the hh and lh transitions comprise an excitonic (X) and a continuum (C) part. For wells that are not too narrow, e.g., $L_z \approx 100$ Å, the exciton peaks have a roughly Gaussian line shape, while broadened 2-D Sommerfeld enhancement profiles describe well the continua contributions [6], [32]. Inasmuch as the confinement potential dominates the motion normal to the layers, it is legitimate to describe the excitons by a wave function separable in the e–h relative coordinate (r) and the e–h coordinates along the normal ($z_{e,h}$); $\psi_{ih,n_z}(z_e, z_h, r) = \phi^e_{n_z}(z)\,\phi^{ih}_{n_z}(z)\,\Phi(r)$ where i = h or l. Then the strength of the exciton absorption is

$$\alpha^{(0)}_{iX,n_z} \propto |p_{cv}|^2 \left|\langle \phi^e_{n_z}(z) | \phi^{ih}_{n_z}(z)\rangle\right|^2 |\Phi(r=0)|^2 \quad (2)$$

where p_{cv} is the usual interband momentum matrix element, assumed to be independent of k. The second factor in (2) describes the overlap of the e and h wave functions perpendicular to the layer. The third factor accounts for the excitonic enhancement which is produced by the increased probability of finding the two particles in the same unit cell.

B. MD-QW's

The absorption spectra of MD-QW's have been much less investigated, and only recently have detailed experimental determinations and theoretical descriptions been achieved. In this subsection, we restrict ourselves to the n-type doping which is used in our experiments, and we shall only review the most salient features. A detailed discussion can be found in [21] and [33]. Obviously, in MD-QW's the occupation of the conduction band produces PSF and many-body effects close to the gap. The carriers will also affect the high-energy states, although less directly, through such effects as collisional broadening. Furthermore, the charge separation produces electrostatic fields that can modify strongly the optical transitions. The electrostatic effects are normally treated in real space [2], [3]. However, the many-body effects must be analyzed in the phase space because the consequences of the Pauli exclusion principle are more naturally expressed in terms of the momentum k, which is a good quantum number in crystals. Therefore, we shall discuss separately the two types of modifications of $\alpha(\hbar\omega)$. We will introduce the most important ideas and sketch the theoretical treatment without getting into details. For the reader interested in these, we will indicate the proper references.

Let us consider how e–h correlation is modified by the presence of a plasma. The excitonic states can be expressed as a linear combination of pair states:

$$|x_n\rangle = \sum_k \Phi_n(k)\, c_e^+(k)\, c_h^+(-k)\,|g\rangle \quad (3)$$

where k is the Fourier conjugate of the e–h relative motion coordinate, $c^+_{e,h}$ are the e and h creation operators, and $|g\rangle$ is the crystal ground state with an empty conduction band and a full valence band. In writing (3), we have assumed that the exciton is photogenerated so that the momentum of the center of mass vanishes, and to simplify the notation, we do not mention spin composition and indexes explicitly. $\Phi_n(k)$ is the exciton wave function in k-space. The corresponding wave function in real space, which has the familiar hydrogenic functional form, is simply the Fourier transform of $\Phi_n(k)$, i.e.,

$$\Phi_n(r) = \sum_k e^{ikr}\Phi_n(k). \quad (4)$$

Both $\Phi_n(r)$ and $\Phi_n(k)$ obey a Schrödinger equation describing the e–h relative motion. The expression of this equation in k-space is [34]

$$E_n\Phi_n(k) = \left[\epsilon_e(k) + \epsilon_h(k)\right]\Phi_n(k) - \sum_{k'} V(k-k')\,\Phi_n(k') \quad (5)$$

where $\epsilon_{e,h}(k) = \pm[E_g/2 + (\hbar^2/2m_{e,h})\,k^2]$ are the single particle e (h) energies and $V(q)$ is the Coulomb potential screened by the static dielectric constant of the material ϵ_0 expressed in k-space. The index n runs over the discrete (bound states) as well as over the continuous (scattering states) spectra. The absorption coefficient including correlation enhancement is given by the interband density of states:

$$\alpha^{(0)}(\hbar\omega) \propto \sum_n \delta(\hbar\omega - E_n) \times \sum_{k,k'} \Phi_n(k)\,\Phi_n^*(k'). \quad (6)$$

The spectrum of $\alpha^{(0)}(\hbar\omega)$ consists of both a Balmer series and a continuum. The correlation is still important in the continuum where it produces the Sommerfeld enhancement. Let us note from (6) that the correlation enhancement factor can also be written as $\Sigma_{k,k'}\,\Phi_n(k)\,\Phi_n^*(k') = |\Phi_n(r=0)|^2$, thus reproducing the familiar form found in (2).

When a density N of charges is introduced in the QW, it produces filling of states and screening. The Coulomb potential becomes $V_s(q) = V(q)/\epsilon(q,\omega)$ where $\epsilon(q,\omega)$ is the new dielectric constant that accounts for the effects of the charges. This induces several modifications of the electronic structure. First, the energies of the single-par-

ticle states are renormalized; $E_{e,h}(k) = \epsilon_{e,h}(k) + \Sigma_{e,h}(k)$. The self energies $\Sigma_{e,h}(k)$ express how the energy of the particles due to their own potential is changed by the presence of the other particles. This concept was already used in classical physics, and the correct quantum mechanical description accounts for the proper modification of the Coulomb interaction due to the exclusion principle, i.e., exchange interaction (EI) and direct screening (DS) [34], [35]. Hence, the gap between the conduction and valence bands shrinks. The bandgap renormalization (BGR) is $\Delta E_g = \Sigma_h(0) + \Sigma_e(0)$. The exact determination of $\Sigma_{e,h}(0)$ and ΔE_g in the QW requires rather elaborate numerical calculations. However, the results of such numerical calculations, performed for the quasi-2-D case of QW's at moderate densities and low temperature [36], [37], have shown that, with a remarkable accuracy, the exchange correlation potential μ_{xc} varies as $\mu_{xc}/R_y^{2\text{-D}} \approx -3.1 \times (Na_{2\text{-D}})^{1/3}$ where $R_y^{2\text{-D}}$ and $a_{2\text{-D}}$ are the 2-D Rydberg and 2-D Bohr radii of the QW material. Recently, high-density PL experiments at the $n_z = 1$ gap of a number of III-V QWS's have indicated that this expression has a rather general character [38], [39] in close analogy with a similar one in 3-D [40].

It is not known, however, how much the $n_z > 1$ edges are affected by the introduction of carriers at the $n_z = 1$ gap. An idea customarily associated with BGR is that of "rigid band shifts" [34]. Although rigid shifts may occur within a 2-D subband, the intersubband BGR (i.e., the BGR induced by carriers in one subband on another subband) has been found experimentally to be rather small. Observation of the dynamics of the screening in GaAs/AlGaAs's QWS's [41] has shown that when photocarriers are introduced in the $n_z = 1$ continuum, they produce very small intrasubband and intersubband screening as long as they do not occupy the bottom of the $n_z = 1$ subbands. When they have relaxed to the bottom of the $n_z = 1$ subbands, the screening within this subband becomes substantial, but the screening in $n_z = 2$ as measured by the red shift of the $n_z = 2$ optical transition edge remains approximately one order of magnitude smaller than the intrasubband screening. A plausible explanation for such a result is that, conversely to what is commonly assumed, the Coulomb interaction is not constant in k-space. Indeed, QW's within a heterostructure are normally treated as a quasi-2-D system, as shown by all of the above discussion; however, it is always possible to describe the whole heterostructure as a 3-D system if the anisotropy of all properties is properly accounted for. In particular, for the electronic states which are confined within the QW, the 3-D wave vector K can be written $K = (k_z, k)$ where k is the 2-D wave vector considered so far and the "perpendicular wave vector" k_z is associated the kinetic energy induced by the confinement in the QW. It depends on the subband and varies approximately as $|k_s| \approx \pi n_z/L_z$. In the 3-D k-space, the Coulomb potential varies as $V(q) \propto q^{-2}$ where q is the wave vector mismatch, $q = K - K'$, so that *intersubband screening* is governed by $(|k_z - k_z'|^2 + |k - k'|^2)^{-1}$. Thus, because for states belonging to different subbands $|k_z - k_z'|$ is always large, the intersubband screening is very small, even when $k = k' = 0$. The effects of the dependence of $V(q)$ on the dielectric constant do not affect the validity of the above argument. Intersubband EI is almost completely quenched, and the intersubband DS is strongly reduced. Hence, in MD-QW's the BGR effects are only important close to the fundamental gap, even up to rather large carrier concentrations.

In the vicinity of this gap, the correction due to the BGR in MD-QW's can be derived from the correlation exchange potential μ_{xc} using the fitted analytical expression discussed previously [36], [37] and

$$\Delta E_{BGR} = \frac{1}{2}\frac{\partial}{\partial N}(N\mu_{xc}) \tag{7}$$

where the factor $1/2$ accounts for the fact that there are only electrons in the MD-QW.

Both the change of single-particle energies and the screening must be included in (5), but this is not the only modification to account for. As seen from (3), the reduction of available states due to occupancy will also affect the way the exciton states can be built. The effects of PSF are naturally described by the quantity $F(k) = [1 - f_e(k) - f_h(k)]$. All together, the new Schrödinger equation is [34], [35]

$$E_j\Psi_j(k) = [E_e(k) + E_h(k)]\,\Psi_j(k) - \sum_{k'} \operatorname{sgn}[F(k)] \cdot |F(k)|^{1/2} V_s(k - k')|F(k')|^{1/2}\Psi_j(k'). \tag{8}$$

In the dilute limit ($F(k) \approx 1$), it is found that the eigenenergies E_j still form a discrete spectrum and, of course, a continuous one as well. The states of the discrete spectrum are less tightly bound than in the absence of carriers, $E_j < E_n$, and correspondingly, the correlation is also reduced. For large concentrations, because of the shortage of unoccupied single-particle states out of which excitons are built (PSF) and because of screening (EI + DS), there are no more bound states, and only scattering states exist (i.e., the index j has only a continuous spectrum). However, there is still a nonnegligible e–h correlation in the continuum. The absorption profile in the presence of the plasma can be calculated from this equation using Green's function techniques [35]. In this case, it can be written

$$\alpha^{(N)}(\hbar\omega) \propto \sum_j \delta(\hbar\omega - E_j) \sum_{k,k'} |F(k')|^{1/2} \cdot \Psi_j^*(k')\,|F(k)|^{1/2}\Psi_j(k). \tag{9}$$

By comparing (6) and (9), one sees clearly the changes brought about by the charges present in the material. The energies of the resonances are redshifted, but due to the neutrality of excitons [34] the shifts are larger for the single-particle states than for the bound states (when these exist). The oscillator strengths are reduced for two reasons: first, as a direct consequence of the exclusion principle, as it is expressed by the factors $|F(k)|^{1/2}$, and

second, because of the weaker correlation (i.e., $|\Psi(r=0)| < |\Phi(r=0)|$). For large concentrations, there are no more exciton resonances, and the absorption above the gap is completely quenched over all the range for which $F(k) = 0$. It is not possible to go beyond our general arguments without numerical integration. This has been performed for two-component plasmas [35] and single-component plasmas [21]. However, let us note that it is customarily assumed that the wave functions are the free-particle plane wave functions in the continuum above the $n_z = 1$ excitons. This approximation results in the widely used expression

$$\alpha_C^{(N)}(\hbar\omega) \approx \alpha_C^{(0)}(\hbar\omega) \times [1 - f_e(k) - f_h(k)] \quad (10)$$

where $(\hbar\omega - E_g) = \hbar^2k^2/2m$ and m is the e–h reduced mass ($m^{-1} = m_e^{-1} + m_h^{-1}$). Finally, let us note that, in QW's that are not too wide, the PSF due to electrons at the bottom of the first subband on the higher ones is small for two reasons. First, in such QW's the intersubband separation is large enough to prevent significant occupation of the higher levels even at room temperature. In addition, the states belonging to different subbands are (almost) orthogonal, so that the effects of exclusion are minimized.

The other changes in $\alpha(\hbar\omega)$ of interest here are due to electrostatic fields that can develop along the direction perpendicular to the layers and therefore directly affect the $\phi_{n_z}^{e,h}(z)$ part of the exciton wave function. For undoped QW's without external field applied, these have a sinusoidal dependence inside the well and exponential decaying tails outside. Modification of the absorption when a uniform electrostatic field is applied normal to the layer is now well documented and understood [2], [3]. The wave functions become Airy functions, corresponding to an asymmetric charge distribution in the well. However, because of the large potential steps between the QW material and the barrier material, the tunneling time out of the QW is very long, and the e and h remain confined in the well even at large fields. Hence, for well widths smaller than the bulk exciton Bohr radius ($L_z < a_0$), the e–h correlation remains important, and excitons are still observed even in fields much larger than the 3-D classical ionization field [2]. Nevertheless, both the wave function overlap and the energies are changed. The lowest transitions allowed in the absence of field usually lose strength and are red shifted. By contrast, the "forbidden transitions" appear more clearly and gain strength as the field increases. It can be shown that several sum rules apply, so that the total absorption strength below some energy is conserved [3]. When charges are introduced in the QW by MD, the charge separation produces band-bending effects, which in turn affect the wave functions of the mobile charges, hence changing the field. In order to describe the net variation of the energy levels and wave function overlaps, it is necessary to solve self-consistently the Schrödinger and the Poisson equations [33], [42]. This can be done numerically with great accuracy for the 1-D problem. It is found that the energy shifts are not very large for symmetric charge distributions, but they can become substantial in one-sided MD.

To summarize the discussion of this section, when an electrostatic field is used in an FE-QWS to move carriers into an MD-QW, we can expect the following changes in the absorption spectrum as compared to that of the empty QW. First, for all the subbands, the electrostatic fields will shift the energy levels, reducing the oscillator strength of the allowed transitions and increasing that of the "forbidden" ones. Second, the occupation of the lowest conduction subband will produce quenching of the absorption and renormalization effects at the fundamental gap, but it should not significantly affect the higher subbands.

III. Modulation of Absorption in FE-QWS's

A. Sample Description and Experimental Method

As already mentioned in the Introduction, the high mobility and large density of the 2-D electron gas which are attainable in MD-QW's make these structures very attractive for electronic transport devices [11]. Mobilities $\mu > 10^6$ cm^2/V · s have been observed at low temperature in MD GaAs/AlGaAs single-interface structures. These structures have been used for fundamental investigations, such as the study of quantum Hall effect [12], as well as for applications. In particular, the electron density can be tuned by an electric field applied to the sample, resulting in the changes of the current flow between two electrodes. Modulation-doped field-effect transistors (MODFET's) using this mechanism were demonstrated to operate at high speed and were shown to be capable of driving large currents [43]. Switching times as short as a few picoseconds were obtained with submicrometer gates [44].

The system of InGaAs/InAlAs lattice matched to InP has a number of attractive features for utilization in FE structures. The electron effective mass in InGaAs is low, $m_e = 0.041m_0$. Good Schottky barriers can be formed on InAlAs. High-quality MODFET's have been demonstrated in this material system with sheet carrier densities $N > 10^{12}$ cm^{-2} in the dark [45], [46]. These devices show no persistent photoconductivity and in fact exhibit no significant sensitivity to light. They exhibit good transconductance as high as 270 mS/mm for 1.6 μm gate lengths [46]. QWS's made of these compounds present yet another very important characteristic for our experiments and other optoelectronic applications. The bandgaps of the substrate (E_g(InP) $\approx$ 1.42 eV) and of the barrier material (E_g(InAlAs) $\approx$ 1.55 eV) are significantly larger than that of the InGaAs (E_g(InGaAs) $\approx$ 0.81 eV). In fact, there is a spectral window about 600 nm wide in which only the InGaAs QW's absorb light. This feature offers unique opportunities for photonic–electronic integration because electronic devices, fabricated by conventional processing techniques in epilayers grown onto InP substrates, can be probed optically from beneath through the InP substrate and InAlAs layers. Devices of this category and of particular interest for our experiments are special MODFET's in which the conducting channel containing the 2-D electron gas is an InGaAs QW [22], [23].

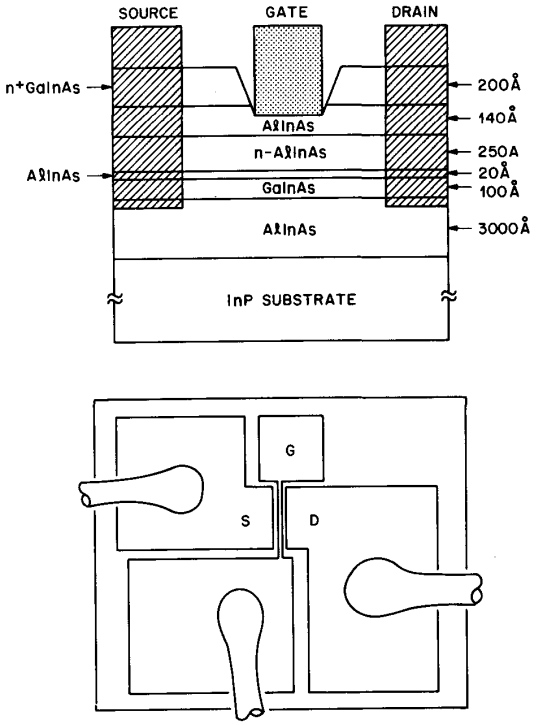

Fig. 1. (a) Structure of an FET. The 100 Å InGaAs layer is undoped, and the InAlAs central layer (250 Å) is doped with Si ~ 1.2×10^{18} cm^{-3}. (b) Top view of the MODFET showing the electrode structure and the extended optical pad.

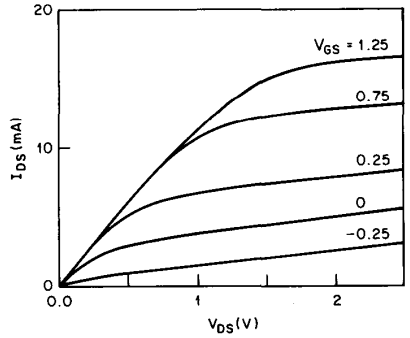

Fig. 2. Typical source-to-drain, $I_{SD}(V)$, characteristics of the InGaAs/InAlAs MODFET for a set of gate voltages.

The structure used in our experiments is shown in Fig. 1(a). The wafers were grown by molecular beam epitaxy (MBE) and prepared using conventional photolithography and lift-off techniques [45], [46]. The epilayers were grown on a (100) Fe-doped semiinsulating InP substrate. They consist first of a 3000 Å undoped $In_{0.52}Al_{0.48}As$ buffer layer, followed by a 110 Å undoped $In_{0.53}Ga_{0.47}As$ QW. To have a better separation between the carriers in the conduction channel (i.e., the electron wave functions in the well) and the impurities in the doped region, a 20 Å undoped $In_{0.52}Al_{0.48}As$ spacer layer separates the QW from a 250 Å $In_{0.52}Al_{0.48}As$ layer doped with Si $\approx 1.2 \times 10^{18}$ cm^{-3}. Finally, a 140 Å undoped $In_{0.52}Al_{0.48}As$ layer and a 200 Å n^+-$In_{0.53}Ga_{0.47}As$ cap layer complete the structure.

Hall measurements indicate that the sample indeed exhibits good low-field mobilities: $\mu = 9.4 \times 10^3$ cm^2/Vs at 300 K and $\mu = 3.7 \times 10^4$ cm^2/V · s at 77 K. The corresponding sheet carrier densities are $N(300\ \text{K}) = 1.79 \times 10^{12}$ cm^{-2} and $N(77\ \text{K}) = 1.6 \times 10^{12}$ cm^{-2}. Fig. 1(b) shows a top view of the MODFET's. The drain and source were made by evaporating and then alloying AuGe/Au, such that an ohmic contact was formed to the conduction channel. The gate area was first recessed 230 Å by a slow chemical etch to remove the n^+ cap layer. The Schottky gate was a 1.6 μm × 100 μm pattern consisting of 300 Å Cr under 3000 Å Au and was centered in a 5.4 μm gap between the source and the drain. It was connected on one side through an air bridge to a bonding pad. The other side of the gate was connected to a 100 μm × 100 μm pad, which served as an active area for optical probing. It should be noted that the electron density at the optical probing pad is the same as under the short gate since they are held at the same potential. Finally, the FET's were isolated by a deep mesa etch.

Fig. 2 shows the drain–source current I_{DS} as a function of the drain–source voltage V_{DS} as the gate–source voltage V_G is varied. These characteristics show the excellent quality of the MODFET's. As expected, one sees clearly that as V_G is decreased, the resistivity of the channel increases and I_{DS} drops. For all the MODFET's processed from this wafer, the pinch-off voltage at which the conducting channel does not conduct any more is found to be approximately $V_\phi \approx -0.5$ V. Fig. 3 illustrates the variations of the band structure in real space below the gate and the corresponding spatial distributions of charges in the MODFET above and below pinch-off. Below pinch-off (lower part of Fig. 3), the Schottky barrier is high, and it pulls the $n_z = 1$ QW confined level above the Fermi energy E_F. The QW is empty, and it has a flat profile. In this condition, conduction is inhibited, and if any current I_{DS} is measured, it originates from leakage (mainly due to the extended gate). As a positive gate voltage is applied, the Schottky barrier is lowered, the $n_z = 1$ QW level is below the E_F, electrons are admitted in the well, and conduction is possible (upper part of Fig. 3). The density of electrons in the QW depends on the position of the $n_z = 1$ level relative to E_F. The charges in the well adjust to minimize the energy, thus producing a nonuniform field, and the QW profile is bent.

For the optical measurements, the samples were mounted on the cold finger of a cryostat, and the lattice temperature T_L could be tuned from 10 to 300 K. The light source consisted of a tungsten lamp and a 0.25 m monochromator with a spectral resolution of ≈4 nm. The exit slit was imaged on the MODFET to form a 100 μm × 100 μm square, which coincided with the optical probing pad. The light from the monochromator was sent through the transparent substrate and reflected off the metal elec-

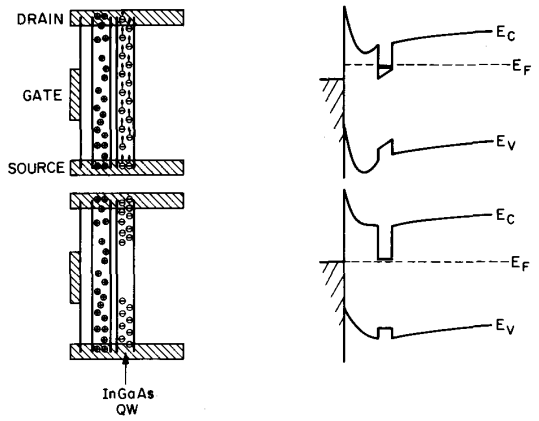

Fig. 3. Schematic of the charge distribution in the MODFET and of the real-space band structure under the gate below and above pinch-off.

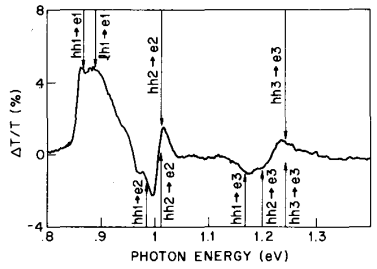

Fig. 4. A typical low-temperature (T_L) differential absorption spectrum. The positions of the calculated energy levels are indicated by the arrows, for the empty QW (top arrows) and the full QW (bottom arrows).

trode, thus passing twice through the QW. Beam splitters, microscopes, IR TV cameras, and detectors were used to image the samples and the IR beam and to measure the reflected light intensities. The use of a tungsten lamp monochromator as a light source enabled us to probe a broad spectral range, from the InAlAs bandgap to the InGaAs bandgap, thus covering the $n_z = 1$, 2, and 3 QW transitions.

The absorption coefficient of an InGaAs/InAlAs QWS near the bandgap is approximately 5000 cm^{-1} [6]; thus, a single 100 Å QW absorbs only ≈ 1 percent of the light. Detecting the variation of such a small absorption requires a sensitive technique. The inherent advantage of the MODFET structure is that it enables us to use lock-in techniques to perform differential measurements with a $\Delta T/T \approx 10^{-4}$ sensitivity. The principle of the measurement is the following. The gate voltage is modulated between two values V_1 and $V_2 = V_1 + \Delta V$ at some frequency f, driving the electron density in the QW between N_1 and $N_2 = N_1 + \Delta N$. This, in turn, modulates the light transmitted through the QW because, according to (9), the absorption coefficient follows the variations of the density changing between $\alpha^{(N_1)}(\hbar\omega)$ and $\alpha^{(N_2)}(\hbar\omega) = \alpha^{(N_1)}(\hbar\omega) + \Delta\alpha(\hbar\omega)$. The component at the frequency f of the relative change in transmission $\Delta T/T$ is then measured using sensitive lock-in amplifiers. For a probe beam making two passes through the QW, one has, in the small signal regime, $\Delta T/T \approx 2L_z\Delta\alpha(\hbar\omega)$. In particular, if V_1 is set to be equal to the pinch-off voltage V_ϕ, the measured signal corresponds to the difference between the absorption of an empty QW, $\alpha^{(0)}(\hbar\omega)$ given by (6), and that of a QW containing N electrons, $\alpha^{(N)}(\hbar\omega)$ given by (9). In all the measurements, V_1 was set to be equal to V_ϕ. We shall call the $\Delta\alpha(\hbar\omega)$ spectra differential absorption spectra (DAS).

It is worth noting that, in this double-pass geometry, a standing wave pattern can form just below the metallic mirror gate. This might lead to some ambiguity in determining the actual intensity in the well and to some spectral distortion due to the shift of the standing wave pattern with changing wavelength. In fact, for practical applications, one may take advantage of this effect to enhance the absorption by positioning the QW at a maximum of the standing wave.

B. Experimental Results

Fig. 4 shows a typical DAS at a temperature $T_L \approx 10$ K. Three broad features are clearly recognized at 0.85, 1, and 1.2 eV. The lower-energy peak occurs at the bandgap of the QW and is a positive signal. The two others have a "derivative line shape" with a negative low-energy side and a positive high-energy side. A positive peak in a DAS corresponds to a spectral region where $\alpha^{(0)}(\hbar\omega) > \alpha^{(N)}(\hbar\omega)$, and vice versa for a negative peak. Therefore, the lowest-energy peak corresponds to the reduction of the absorption near the bandgap as the QW fills up with electrons. The absolute change in the absorption at that region is approximately 4 percent, showing that at this density the absorption is *completely quenched*. At the higher-energy spectral features, the profile is mixed and consists of regions of increased and decreased absorption. One could obtain such a behavior from shifts and broadening of resonances. It is also interesting to note that the three peaks are separated by flat regions, where essentially no change of the absorption occurs.

Fig. 5 shows a set of DAS for a series of increasing ΔV also taken at $T_L \approx 10$ K. The evolution of the DAS, as the QW is progressively filled with electrons, is easily followed. The signal at the bandgap starts with a symmetric line shape and increases in height until $\Delta V = 0.5$ V (spectra 1–3). Above this voltage, the height of the peak reaches a maximum, and it stops growing as two distinct exciton resonances appear. The peak then broadens asymmetrically, the low-energy side remaining constant while the high-energy side extends (spectra 4–5). At the other two spectral features, no saturation is seen, and both the positive and the negative peaks increase with ΔV. However, the negative peaks develop extra shoulders that become very clear in the last two DAS (spectra 4 and 5).

The room-temperature behavior is shown in Fig. 6. The same three spectral features are also observed, with similar characteristics and evolution. The whole spectra are shifted to low energy, and the maximum change in signal is smaller, $\Delta T/T \approx 2$ percent, reflecting the usual tem-

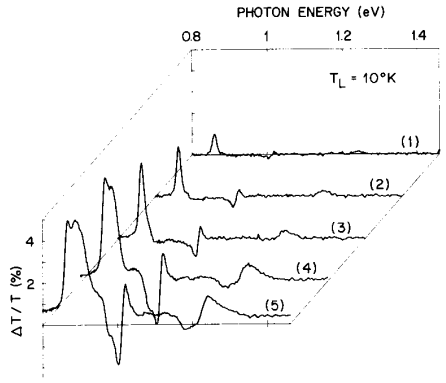

Fig. 5. Set of DAS at $T_L \approx 10$ K. Spectra 1 to 5 correspond to gate-source voltage modulation between pinch-off ($V_\phi = -0.5$ V) and $V_g = -0.2$, -0.1, 0, $+0.5$, and $+1$ V, respectively.

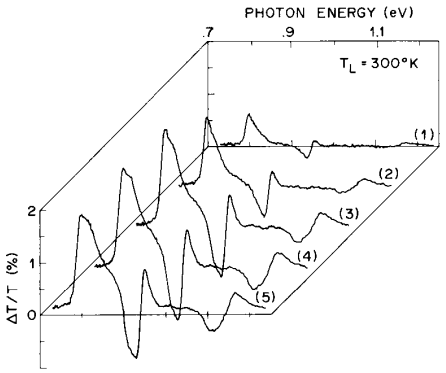

Fig. 6. Set of DAS at $T_L \approx 300$ K. Spectra 1 to 5 correspond to gate-source voltage modulation between pinch-off ($V_\phi = -0.5$ V) and $V_g = -0.2$, -0.0, $+0.5$, $+1$, and $+1.5$ V, respectively.

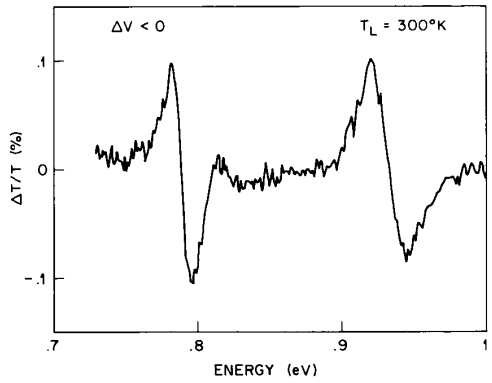

Fig. 7. DAS at $T_L \approx 300$ K for $\Delta V < 0$ corresponding to the normal QCSE in an empty QW. The DAS shown was obtained for a modulation of the gate-source voltage between pinch-off ($V_\phi = -0.5$ V) and $V_G = -1.5$ V.

perature dependence of the gaps and the reduction of absorption at high temperature. The broadening of the peaks is especially important at the low-energy peak, which at large ΔV becomes very asymmetric, with a relatively long tail at the high-energy side.

The DAS are significantly changed as we go to negative ΔV, i.e., $V_2 < V_\phi$. Fig. 7 shows the room-temperature DAS of $\Delta V < 0$. The first noticeable change is the shape of the first spectral feature at the $n_z = 1$ transition, which now has a differential line shape similar to the high-energy ones. Comparison to Fig. 5 reveals that at this energy the DAS signal changes signs exactly at the low-energy edge of the DAS of $\Delta V > 0$ (note the different energy scales on the two figures). We find that the $\Delta T/T \approx 0.1$ percent is significantly smaller.

In order to be able to assign the different features observed in the DAS, we performed room-temperature photoconductivity-excitation measurements. We used the same experimental apparatus, but this time applied a small voltage between the drain and the source of the MODFET. The incident light was chopped, and the I_{DS} was measured by a lock-in amplifier. Unlike in a direct absorption measurement, the line shape is distorted and may change with the applied gate voltage. However, for the assignment of the transition energies, this measurement proves to be useful. Fig. 8 shows the photocurrent as a function of photon energy for a nearly empty well (solid line) and for a partially full well (dashed line). It is seen without ambiguity that the three spectral features discussed above occur at the $n_z = 1$, 2, and 3 transitions. Fig. 8 also confirms that as the QW is filled the absorption is quenched near the $n_z = 1$ transition. It is also seen that the $n_z = 2$ resonance is broadened and red shifted, whereas $n_z = 3$ disappears almost completely.

IV. Interpretation and Discussion of the Experimental Results

In this section, we analyze the results presented in the previous section using the formalism introduced in Section II. We start by solving the Schrödinger equation for the empty well and obtain the transition energies. We then step forward to find the transition energies and line shape of the full well. As was already shown in Section II, we expect the behavior at the first intersubband transition to be significantly different from that at the higher ones. Hence, this part of the analysis is divided in two: the first part deals with the $n_z = 1$ subband, and the second part deals with the $n_z = 2$ and 3 subbands.

We start by reconstructing the absorption spectrum of the empty QW. This is done by determining numerically the single-particle energy levels of the QW and the excitonic binding energies associated with the optical transitions [1], [2]. For this calculation, the band offsets between the QW and barrier material that we have used are $\Delta E_c = 0.60 \times \Delta E_g = 440$ meV and $\Delta E_v = 0.40 \times \Delta E_g = 293$ meV for the conduction and valence bands, respectively [6], [47]. For the masses of the e, hh, and lh, we took $m_e = 0.041\ m_0$, $m_{hh} = 0.377 m_0$, and $m_{lh} = 0.0516 m_0$ in the QW, and $m_e = 0.071 m_0$, $m_{hh} = 0.58 m_0$, and $m_{lh} = 0.14 m_0$ in the barrier material. The positions of the $n_z = 1$, 2, and 3 transitions are indicated as the top

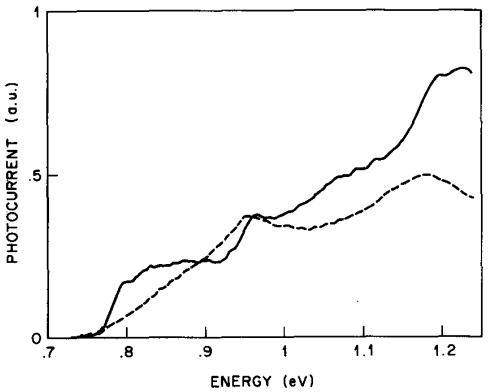

Fig. 8. Room-temperature photocurrent spectra for a nearly empty well (solid line) and for a full well (dashed line).

arrows in Fig. 4. They correspond very well to the positive peaks of the DAS. Again, we note that there are flat regions between these transitions where the continuum absorption is not modified in the full QW. At the $n_z = 1$ transition, the hh and lh excitons are identified. The fact that these excitons are observed confirms that at the pinch-off voltage the QW is indeed completely empty at this temperature.

The transitions of the full well are more difficult to determine since the $\alpha^{(N_1)}(\hbar\omega)$ spectrum involves both electrostatic and many-body effects. First, the single-particle states of a full QW are displaced by the electrostatic potential originating from the gate voltage V_G and from the spatial separation of the negative (electrons in the QW) and the positive (ionized donors in the barrier) charges. The charge densities, which can be large ($> 10^{11}$ cm^{-2}), give rise to a significant band bending. Furthermore, as discussed in Section I, the presence of a Fermi sea of electrons induces a number of many-body effects (PSF, EI, and BRG). In order to account as much as possible for all these effects and interpret our data, we proceed as follows. We solve self-consistently Poisson and Schrödinger equations for the QW containing N electrons and determine the new single-particle states. We then calculate the BGR associated with this electron density. Finally, we determine the effects of PSF. We can then obtain the absorption line shape of the full QW, which can be compared to experiments.

In the self-consistent calculation, the Schrödinger equation is solved numerically using a tunneling resonance program. For the first iteration, we distribute all electrons in the lowest conduction-band level E_1 according to spatial distribution, $|\phi_e^{(0)}|^2$. This approach is correct for low temperatures and for concentrations such that the Fermi level E_F is below the second confined level. At $T = 10$ K and $N < 3 \times 10^{11}$ cm^{-2}, both conditions are satisfied. Assuming the N positive donors to be uniformly distributed throughout the doped region of the barrier, the Poisson equation is then solved to find the electrostatic potential corresponding to this charge distribution, which is then added to the square-well potential. In the next iterations, the free-electron gas is allowed to respond to this potential: the Schrödinger equation solved again, the electrons are redistributed according to the square of the new wave function, and the process is repeated. The single-particle energies for the electrons converged rapidly: five iterations are enough to give convergence within 0.5 meV. We used the results of the last iteration for the final distribution of electrons in the QW, and consequently for the final electrostatic potential, which, added to the square-well potential, determined the final potential profile in which the hh and lh single-particle states were calculated. We denote this correction to the transition energies, which originates from the QCSE, as ΔE_{QCSE}.

In the vicinity of the gap, the correction resulting from the BGR is given by (7). Taking $a_{2\text{-D}} = 190$ Å and $R_y = 2.8$ meV for InGaAs, we obtain $\Delta E_{\mathrm{BGR}} \approx -0.9 \times 10^{-3} N^{1/3}$ where N is expressed per square centimeter and ΔE_{BGR} is in millielectronvolts. The shift introduced by this mechanism is relatively small, and it is also a slowly varying function of N. Typical values of interest for our discussion are in the range 4.1 meV $< \Delta E_{\mathrm{BGR}} <$ 8.6 meV for 10^{11} cm$^{-2} < N < 10^{12}$ cm^{-2}. Thus, the corrections for the BGR are not very important, especially when compared to PSF, which close to the gap dominates over a range on the order of E_F.

Let us now discuss the DAS line shape near the first transition. In Fig. 9, we show a schematic of the band structure. The solid line represents the $n_z = 1$ conduction subband in the presence of N electrons ($E_c(N)$), i.e., including the QCSE and the BGR shifts, and the dashed line represents that of the empty well ($E_c(0)$). The band-to-band transitions are $E_{11}(N)$ and $E_{11}(0)$, respectively, with

$$E_{11}(N) = E_{11}(0) - \Delta E_{\mathrm{QCSE}}(N) - \Delta E_{\mathrm{BGR}}(N). \quad (11)$$

However, because the electrons fill the states at the bottom of the subband, the threshold for the optical transition is, at $T_e = 0$ K,

$$\hbar\omega_F = E_{11}(N) + \frac{m_e}{m} E_F \quad (12)$$

as indicated by the right-hand arrow in Fig. 9. At a finite temperature, the electrons have a Fermi distribution with a large occupation at the bottom of the subband and a smaller occupation around E_F. Hence, the absorption is completely quenched only near the gap and exhibits a thermal tail at high energy. As soon as E_F becomes larger than the exciton binding energy, the states out of which the excitons are built are occupied, and the resonances disappear [2], [8]. Correlation singularities may appear near the Fermi energy [21]. They are seen only when the impurity scattering has been completely eliminated, for example, in samples with wide spacer. In our sample, the spacer is thin (20 Å) so that there is a substantial penetration of the QW wave function in the doped region. In this case, the Fermi edge singularities are not observed and we will neglect them. In the flat part of the continuum where (10) is valid, the profile of the high-energy side of the DAS is described by

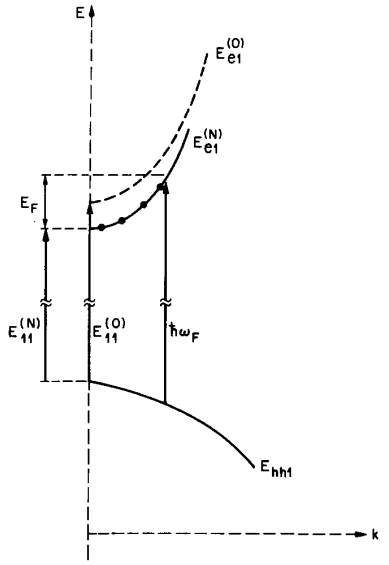

Fig. 9. Schematic band structure near the gap, showing the interband transitions for the empty and full QW and the effect of the conduction subband occupation.

$$\hbar\omega = E_{11}(N) + \hbar^2 \frac{k^2}{2m}.$$

where

$$\Delta\alpha(\hbar\omega) \approx \alpha_C^{(0)}(\hbar\omega) f_e(\hbar\omega) \qquad (13)$$

It should be noted that the complexity of the valence-band structure is not very important since the reduced mass m is primarily governed by the electron mass.

Fitting the DAS profile to the functional form of (13) determines E_F and T_e. Fig. 10 shows a set of DAS blown up in this region of the spectrum, together with the fitted Fermi distribution. The two fitting parameters act independently on the position and shape of the Fermi function, thus giving an easy and unique fit. We find that as long as the gate Schottky diode is reverse-biased and the leakage current is low, $T_e \approx$ constant $\approx$ 50 K, but as the diode is forward-biased the leakage current increases, and T_e rises, up the 120 K. Heating the lattice is easily ruled out from the position of the front edge of $\Delta\alpha(\hbar\omega)$, which does not change. The heating of the 2-D electron gas above T_L is in good agreement with the energy loss rate per carrier in our QW material deduced from the leakage current [48]. The electron density can be deduced from E_F and T_e. Table I summarizes the measured absorption edges $\hbar\omega_F$ at T_L = 10 K and the corresponding Fermi energies, electron densities, and temperatures.

In order to check these results, we performed a room-temperature measurement of the capacitance between the gate and the source as a function of V_G. This technique is customarily used to measure the charge in the FET conduction channel [49]. The leakage current through the gate limits this measurement to the voltage range at which the Schottky diode is reverse-biased. Nevertheless, in the

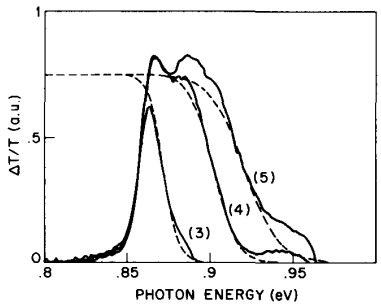

Fig. 10. DAS line shape close to the n_z = 1 transition for the curves 3 to 5 of Fig. 5 and Fermi distribution fitted to the high-energy tails. The temperature and concentration determined by the method described in the text are (3) T_e = 50 K, $N \cong 8 \times 10^{10}$ cm^{-2}; (4) T_e = 80 K, $N \approx 4.3 \times 10^{11}$ cm^{-2}; (5) T_e = 120 K, $N \approx 6.4 \times 10^{11}$ cm^{-2}.

TABLE I
MODULATION OF THE GATE-SOURCE VOLTAGE, FERMI DISTRIBUTION PARAMETERS, AND ELECTRON DENSITIES FOR THE FIVE SPECTRA OF FIG. 5

ΔV	$\hbar\omega_F$	T_e	E_F	N
0.3V	858 meV	50K	-7meV	1.3×10^{10} cm^{-2}
0.4V	866 meV	50K	-1meV	4.2×10^{10} cm^{-2}
0.5V	872 meV	50K	+2meV	8×10^{10} cm^{-2}
1.0V	902 meV	80K	+25meV	4.3×10^{11} cm^{-2}
1.5V	920 meV	120K	+37meV	6.4×10^{11} cm^{-2}

condition where the electrical measurement was possible, the agreement between the two determinations is good: $N(V = 0) = (3.3 \pm 0.4) \times 10^{11}$ cm^{-2} from the $C(V)$ measurement and $N(V = 0) = (3.2 \pm 0.2) \times 10^{11}$ cm^{-2} from the optical measurement.

Now that we know the electron density associated with each DAS spectrum, we can proceed to analyze the DAS near the n_z = 2, 3 subbands. Since the PSF and the BGR are not important there, we use the single-particle levels determined by the self-consistent solution of the Poisson and Schrödinger equations for these charge densities. The corresponding transition energies are shown in Fig. 4 as bottom arrows. The main effects are the shifts ΔE_{QCSE} of the allowed transitions and the appearance of new transitions, previously forbidden. At this point, no broadening has been accounted for, yet the results of the calculations are quite close to the negative peaks of the DAS. The positions of the "forbidden transitions," hh1 → e2, hh1 → e3, and hh2 → e3, which become allowed when the symmetry is broken, correspond very nicely to the negative shoulders which develop with increasing V_G. The new positions of the allowed n_z = 2 and 3 transitions are only slightly below the maximum of the negative peaks. However, an electrostatic broadening [2], or a plasma-colli-

sional broadening [1] of the higher resonances, can account for the small residual offset of the negative peaks. Let us note that the room-temperature photocurrent spectra indeed exhibit a significant broadening. This shows that the electrostatic effects alone describe pretty well the behavior away from the gap. In fact, this also shows that direct information on the electrostatic potential in the QW can be spectroscopically obtained from the DAS.

Finally, we briefly comment on the DAS seen for negative ΔV, shown in Fig. 7. As the bias on the gate is further reversed, beyond the pinch-off voltage, the QW remains empty, but is skewed due to the electrostatic field. This produces a red shift of the various transitions, as seen in the normal QCSE of undoped QW [2]. The signature of such a shift on the DAS is a positive peak at the pinch-off position of the hh exciton and a negative peak at its red-shifted position, which is indeed observed in the experiment.

V. Conclusions

We have shown in previous sections that the DAS techniques provide a new spectroscopic tool to gain important information on the 2-D electron gas in FE-QWS's. The line shape of the first DAS transition determines the density and temperature of the 2-D electron gas, and the position of the negative peaks of the DAS at the higher transition determines the electrostatic potential in the channel. We would like to conclude by discussing briefly how the FE control of the density of the 2-D electron gas can be used for optoelectronic applications such as light modulation, optical interconnects, and optical sampling.

The total absorption quenching which occurs in a MODFET conduction channel may yield both a very large on–off ratio and a very low insertion loss in lightwave modulators. Another attractive property is the broad spectral range ($\approx E_F$) over which light can be modulated. Even though total quenching is attainable only near the bandgap, large modulation can be observed over ≈ 80 meV (>1200 Å) around the bandgap ($\lambda \approx 1.5$ μm) and over a narrower range near the $n_z = 2, 3$ transitions ($\lambda \approx 1.3$ and 1.1 μm). Recently, it has been proposed to exploit this effect in waveguide modulators to increase the interaction length [50].

We have also evaluated the refractive index change in the QW Δn, which is associated with the absorption change $\Delta\alpha$, through a Kramers–Kronig analysis. We have found that it can be very large and may reach $\Delta n \approx 0.1$ below the bandgap. This large refractive index change is especially important for normal incidence phase modulator applications.

Optical interconnects in microelectronics have been intensively considered in the last few years as an alternative to electronic links. One of their attractive advantages is that parallel noninteracting connections can be made. The switching of the transmitted light intensity through a MODFET, which accompanies the switching of the gate voltage, might be important in this context. A reflected beam from the metal gate can be directed to a detector in another position on the board, thus forming an optical interconnection. By designing the structure such that the QW is $\lambda/4n_0$ from the metal gate, where n_0 is the InAlAs refractive index, we can take advantage of the standing wave formed between the incident and the reflected beams and double the transmission change for a double pass to $\Delta T \approx 4$ percent.

The dynamics of extremely fast switching can be followed using an optical sampling technique [51]. Probing above the bandgap is even easier than in the interconnect case and requires much less intensity on the gate. Moreover, the large index change generated at the spectral region below the gap, can be used to perform below-gap sampling.

These examples, of light modulation and transistor logic state readout, demonstrate the uniqueness of the electrical control of carrier concentration in FE-QWS's as a built-in optoelectronic integration. The same device exhibits at the same time excellent electronic and optical performance.

References

[1] For a recent review, see D. S. Chemla and D. A. B. Miller, "Room-temperature excitonic nonlinear-optical effects in semiconductor quantum-well structures," *J. Opt. Soc. Amer.*, vol. B2, pp. 1155–1173, 1985; see also, D. S. Chemla, S. Schmitt-Rink, and D. A. B. Miller, "Nonlinear optical properties of semiconductor quantum wells," in *Optical Nonlinearities and Instabilities in Semiconductors*, H. Haug, Ed. New York: Academic, 1988.

[2] D. A. B. Miller, D. S. Chemla, T. C. Damen, A. C. Gossard, W. Wiegmann, T. H. Wood, and C. A. Burrus, "Electric field dependence of optical absorption near the band gap of quantum well structures," *Phys. Rev.*, vol. B32, pp. 1043–1060, 1985; see also, D. A. B. Miller, D. S. Chemla, and S. Schmitt-Rink, "Electric field dependence of optical properties of semiconductor quantum wells: Physics and applications," in *Optical Nonlinearities and Instabilities in Semiconductors*, H. Haug, Ed. New York: Academic, 1988.

[3] D. A. B. Miller, J. S. Weiner, and D. S. Chemla, "Electric field dependence of linear optical properties in quantum well structures: Waveguide electroabsorption and sum rules," *IEEE J. Quantum Electron.*, vol. QE-22, p. 1816, 1986.

[4] R. C. Miller, and D. A. Kleinmann, "Excitons in GaAs quantum wells," *J. Luminescence*, vol. 30, pp. 530–540, 1985.

[5] D. A. B. Miller, D. S. Chemla, P. W. Smith, A. C. Gossard, and W. T. Tsang, "Room temperature saturation characteristics in GaAs-AlGaAs multiple quantum well structures and of bulk GaAs," *Appl. Phys.*, vol. B28, pp. 96–97, 1982.

[6] J. S. Weiner, D. S. Chemla, D. A. B. Miller, T. H. Wood, D. Sivco, and A. Y. Cho, "Room temperature excitons in 1.6 μm band-gap GaInAs–AlInAs quantum well," *Appl. Phys. Lett.*, vol. 46, pp. 619–621, 1985.

[7] H. Temkin, M. B. Panish, P. M. Petroff, R. A. Hamm, J. M. Vandenberg, and S. Sunski, "GaInAs(P)/InP quantum well structure grown by gas source molecular beam epitaxy," *Appl. Phys. Lett.*, vol. 47, pp. 394–396, 1985.

[8] S. Schmitt-Rink, D. S. Chemla, and D. A. B. Miller, "Theory of the excitonic optical nonlinearities in semiconductor quantum-well structures," *Phys. Rev.*, vol. B32, pp. 6601–6609, 1985.

[9] D. A. B. Miller, D. S. Chemla, and S. Schmitt-Rink, "Relation between electroabsorption in bulk and in quantum wells: The quantum-confined Franz–Keldysh effect," *Phys. Rev.*, vol. B33, pp. 6876–6982, 1986.

[10] H. L. Stormer, R. Dingle, A. C. Gossard, W. Wiegmann, and M. D. Sturge, "Two-dimensional electron gas at differentially doped GaAs-$Ga_{1-x}Al_xAs$ heterojunction interface," *J. Vac. Sci. Technol.*, vol. 16, pp. 1517–1519, 1979; see also, H. L. Stormer, "Electron mobilities in modulation-doped GaAs-(AlGa)As heterostructures," *Surface Sci.*, vol. 132, pp. 519–526, 1983.

[11] A. C. Gossard and A. Pinczuk, "Modulation-doped semiconductors," in *Synthetic Modulated Structures*, L. L. Chang, Ed. New York: Academic, 1985.

[12] D. C. Tsui and H. L. Stormer, "The fractional quantum Hall effect," *IEEE J. Quantum Electron.*, vol. QE-22, pp. 1711-1719, 1986.
[13] A. Pinczuk, J. Shah, R. C. Miller, A. C. Gossard, and W. Wiegmann, "Optical processes of 2-D electron plasma in GaAs/AlGaAs heterostructures," *Solid State Commun.*, vol. 50, pp. 735-739, 1984.
[14] M. H. Meynadier, J. Orgonasi, J. A. Brum, G. Bastard, M. Voos, G. Weimann, and W. Schlapp, "Spectroscopy of a high-mobility GaAs-$Ga_{1-x}Al_xAs$ one-side modulation-doped quantum well," *Phys. Rev.*, vol. B34, pp. 2482-2485, 1986.
[15] C. Delalande, J. Orgonasi, M. H. Meynadier, J. A. Brum, G. Bastard, G. Weimann, and W. Schlapp, "Band gap renormalization in GaAs-$Ga_{1-x}Al_xAs$ modulation doped quantum well," *Solid State Commun.*, vol. 59, pp. 613-617, 1986.
[16] R. Sooryakumar, D. S. Chemla, A. Pinczuk, A. C. Gossard, W. Wiegmann, and L. J. Sham, "Valence band mixing in GaAs-(AlGa)As heterostructures," *Solid State Commun.*, vol. 54, pp. 859-862, 1985.
[17] R. Sooryakumar, A. Pinczuk, A. C. Gossard, D. S. Chemla, and L. J. Sham, "Tuning of the valence-band structure of GaAs quantum wells by uniaxial stress," *Phys. Rev. Lett.*, vol. 58, pp. 1150-1153, 1987.
[18] B. Roulet, J. Gavoret, and P. Nozieres, "Singularities in the X-ray absorption and emission of metals. I. First order parquet calculations," *Phys. Rev.*, vol. 178, pp. 1072-1083, 1969; "Singularities in the X-ray absorption and emission of metals. II. Self-consistent treatment of divergences," *Phys. Rev.*, vol. 178, pp. 1084-1096, 1969; "Singularities in the X-ray absorption and emission of metals. III. One-body theory exact solution," *Phys. Rev.*, vol. 178, pp. 1097-1107, 1969.
[19] A. E. Ruckenstein, S. Schmitt-Rink, and R. C. Miller, "Infrared and polarization anomalies in the optical spectra of modulation-doped semiconductor quantum well structures," *Phys. Rev. Lett.*, vol. 56, pp. 504-507, 1986.
[20] M. S. Skolnick, J. M. Rorison, K. J. Nash, D. J. Mowbray, P. R. Tapster, S. J. Bass, and A. D. Pitt, "Observation of a many-body edge singularity in quantum well luminescence spectra," *Phys. Rev. Lett.*, vol. 58, pp. 2130-2133, 1987.
[21] G. Livescu, D. A. Miller, and D. S. Chemla, "Electron-hole singularities in optical spectra of modulation doped GaAs-AlGaAs quantum well," *Superlattices Microstructures*, 1988, to be published.
[22] D. S. Chemla, I. Bar-Joseph, C. Klingshirn, D. A. B. Miller, J. M. Kuo, and T. Y. Chang, "Optical reading of field-effect transistors by phase-space absorption quenching in a single InGaAs quantum well conducting channel," *Appl. Phys. Lett.*, vol. 50, pp. 585-187, 1987.
[23] I. Bar-Joseph, J. M. Kuo, C. Klingshirn, G. Livescu, D. A. B. Miller, T. Y. Chang, and D. S. Chemla, "Absorption spectroscopy of the continuous transition from low to high electron density in a single modulation-doped InGaAs quantum well," *Phys. Rev. Lett.*, vol. 59, pp. 1357-1360, 1987.
[24] C. Delalande, J. Orgonasi, J. A. Brum, G. Bastard, and M. Voos, "Optical studies of a GaAs quantum well based field-effect transistor," *Appl. Phys. Lett.*, vol. 51, pp. 1346-1348, 1987.
[25] C. Delalande, G. Bastard, J. Orgonasi, J. A. Brum, H. W. Liu, and M. Voos, "Many-body effects in a modulation-doped semiconductor quantum well," *Phys. Rev. Lett.*, vol. 59, pp. 2690-2692, 1987.
[26] G. Bastard, E. E. Mendez, L. L. Chang, and L. Ezaki, "Exciton binding energy in quantum wells," *Phys. Rev.*, vol. B26, pp. 1974-1979, 1982.
[27] R. L. Greene, K. K. Bajaj, and D. E. Phelps, "Energy levels of Wannier excitons in GaAs-AlGaAs quantum well structures," *Phys. Rev.*, vol. B29, pp. 1807-1812, 1984.
[28] M. Shinada and S. Sugano, "Interband optical transitions in extremely anisotropic semiconductors," *J. Phys. Soc. Japan*, vol. 21, pp. 1936-1946, 1966.
[29] Y. C. Chang and J. N. Schulman, "Modification of optical properties of GaAs-$Ga_{1-x}Al_xAs$ superlattices due to band mixing," *Appl. Phys. Lett.*, vol. 43, pp. 536-539, 1983.
[30] U. Ekenberg and M. Altarelli, "Calculation of hole subbands at GaAs-$Ga_{1-x}Al_xAs$ interface," *Phys. Rev.*, vol. B30, pp. 5369-3572, 1984.
[31] D. A. Broido and L. J. Sham, "Effective masses of holes at GaAs-AlGaAs heterojunction," *Phys. Rev.*, vol. B31, pp. 888-892, 1985.
[32] D. S. Chemla, D. A. B. Miller, P. W. Smith, A. C. Gossard, and W. Weigmann, "Room temperature excitonic nonlinear absorption and refraction in GaAs/AlGaAs multiple quantum well structures," *IEEE J. Quantum Electron.*, vol. QE-20, pp. 265-275, 1984.
[33] G. Livescu, D. A. Miller, D. S. Chemla, M. Ramaswamy, T. Y. Chang, N. Sauer, A. C. Gossard, and J. H. English, "Free carrier and many-body effects in absorption spectra of modulation-doped quantum wells," *IEEE J. Quantum Electron.*, this issue, pp. 1677-1689.
[34] For a recent review of semiconductor optical nonlinearities close to the bandgap, see H. Haug and S. Schmitt-Rink, "Electron theory of the optical properties of laser excited semiconductors," *Progr. Quantum Electron.*, vol. 9, pp. 3-100, 1984.
[35] S. Schmitt-Rink, C. Ell, and H. Haug, "Many-body effects in the absorption, gain and luminescence spectra of semiconductor quantum well structures," *Phys. Rev.*, vol. B33, pp. 1183-1189, 1986.
[36] S. Schmitt-Rink and C. Ell, "Excitons and electron-hole plasma in quasi-two-dimensional systems," *J. Luminescence*, vol. 30, pp. 585-596, 1985.
[37] D. A. Kleinmann and R. C. Miller, "Band-gap renormalization in semiconductor quantum wells containing carriers," *Phys. Rev.*, vol. B32, pp. 2266-2272, 1985.
[38] G. Trankle, H. Leier, A. Forchel, H. Haug, C. Ell, and G. Weimann, "Dimensionality dependence of band gap renormalization in two- and three-dimensional electron-hole plasmas in GaAs," *Phys. Rev. Lett.*, vol. 58, pp. 419-422, 1987.
[39] G. Trankle, E. Lach, A. Forchel, H. Haug, C. Ell, G. Weimann, G. Griffiths, H. Kroemer, and S. Subbanna, "Universal relation between band renormalization and carrier density in two-dimensional electron-hole plasmas," *J. Physique*, vol. c5-1987, pp. 385-389, 1987.
[40] P. Vashista and R. K. Kalia, "Universal behavior of exchange-correlation energy in electron-hole liquid," *Phys. Rev.*, vol. B25, pp. 6492-6495, 1982.
[41] W. H. Knox, C. Hirlimann, D. A. B. Miller, J. Shah, D. S. Chemla, and C. V. Shank, "Femtosecond excitation of nonthermal carrier populations in GaAs quantum wells," *Phys. Rev. Lett.*, vol. 56, pp. 1191-1193, 1986.
[42] K. Inoue, H. Sakaki, J. Yosino, and T. Hotta, "Self-consistent calculation of electronic states in AlGaAs/GaAs/AlGaAs selectively doped double heterostructures under electric fields," *J. Appl. Phys.*, vol. 58, pp. 4277-4281, 1985, and references therein.
[43] T. J. Drummond, W. T. Masselink, and H. Morkoc, "Modulation-doped GaAs/AlGaAs heterojunction field-effect transistors: MODFETs," *Proc. IEEE*, vol. 74, pp. 773-821, 1986.
[44] N. J. Shah, S. S. Pei, C. W. Tu, and R. C. Tiberio, "Gate-length dependence of the speed of SSI circuits using submicrometer selectively doped heterostructure transistor technology," *IEEE Trans. Electron Devices*, vol. ED-33, pp. 543-547, 1986.
[45] J. M. Kuo, B. Lalevic, and T. Y. Chang, "New pseudomorphic MODFETs utilizing $Ga_{0.47}In_{53}As/Al_{0.48}In_{0.52}As$ heterostructures," in *Tech. Dig. Int. Electron. Devices Meet. (IEDM)*, Los Angeles, CA, 1986, pro. pp. 460-463.
[46] J. M. Kuo, B. Lalevic, A. Ourmazd, T. Y. Chang, J. L. Zyskind, and J. W. Sulkoff, "Molecular beam epitaxial growth and characterization of $Ga_{0.47-u}In_{53+u}As/Al_{0.48+u}In_{0.52-u}As$ semiconductor-based heterostructures: Interfacial structures and stability," in *Proc. 1986 Northeast Regional Meet. TMS*, Murray Hill, NJ, May 1, 2, 1986.
[47] M. S. Skolnick, P. R. Tapster, S. J. Bass, A. D. Pitt, N. Apsley, and S. P. Aldred, "Investigation of InGaAs-InP quantum wells by optical spectroscopy," *Semicond. Sci. Technol.*, vol. 1, pp. 29-40, 1986.
[48] J. Shah, "Hot carriers in quasi-2D polar semiconductors," *IEEE J. Quantum Electron.*, vol. QE-22, pp. 1728-1743, 1986.
[49] L. P. Sadwick and K. L. Wang, "A treatise on capacitance-voltage relation of high electron mobility transistors," *IEEE Trans. Electron Devices*, vol. ED-33, pp. 651-663, 1986.
[50] A. Kastalsky, J. H. Abeles, and R. F. Leheny, "Novel optoelectronic single quantum well devices based on electron bleaching of exciton absorption," *Appl. Phys. Lett.*, vol. 50, pp. 708-710, 1987.
[51] J. M. Wisenfeld, R. S. Tucker, A. Antreasyan, C. A. Burrus, A. J. Taylor, V. D. Mattera, and P. A. Garbinski, "Electronic sampling measurement of high speed InP integrated circuits," *Appl. Phys. Lett.*, vol. 50, pp. 1310-1312, 1987.

D. S. Chemla (M'84) was born in Tunis, Tunisia, on July 21, 1940. He graduated from the Ecole National Superieure des Telecommunications, Paris, France, in 1965, and received the Doctorat Es-Sciences from the Faculty of Sciences at Paris in 1972.

From 1965 to 1967 he worked at the College de France in high-energy physics. From 1967 to 1981 he worked at the Centre National de'Etudes des Telecommunications at an MTS Group Leader and Department Head. He joined AT&T Bell Lab-

oratories, Holmdel, NJ, in 1981 and is now head of the Quantum Physics and Electronic Research Department. He has been engaged in research on nonlinear optics of insulators, organic molecules, and crystals and semiconductors. He is currently interested in the optical response of microstructures under excitation by ultrashort and high intensity light pulses.

I. Bar Joseph, photograph and biography not available at the time of publication.

J. M. Kuo, photograph and biography not available at the time of publication.

T. Y. Chang (S'62-M'70), for a photograph and biography, see this issue, p. 1689.

C. Klingshirn, photograph and biography not available at the time of publication.

Gabriela Livescu, for a photograph and biography, see this issue, p. 1689.

David A. B. Miller was born in Hamilton, UK in 1954. He received the B.Sc. degree from St. Andrews University, UK, in 1976 and the Ph.D. degree in physics from Heriot-Watt University, UK, in 1979.

He continued working with the Physics Department at Heriot-Watt, latterly as a lecturer. He joined AT&T Bell Laboratories in Holmdel, NJ, in 1981, and has been Head of the Photonics Switching Device Research Department since 1987. His research interests include optical properties of quantum-confined structures and optical logic and switching devices.

Dr. Miller is a member of the Optical Society of America and the American Physical Society. He received the Adolph Lomb Medal of the Optical Society of America for contributions to semiconductor nonlinear optics, and is a R. W. Wood Metal co-recipient for his work on quantum wells. He has also been an IEEE-Lasers and Electro-Optics Society Traveling Lecturer.